Journal of Power Sources 246 (2014) 141–148

Contents lists available at ScienceDirect

Journal of Power Sources

journal homepage: www.elsevier.com/locate/jpowsour

Changes in the mechanical properties of support materials for segmented-in-series type solid oxide fuel cells as a function of time

T. Somekawa*, Y. Matsuzaki

Fundamental Technology Dept., Tokyo Gas Co., Ltd., 1-7-7, Suehiro-cho, Tsurumi-ku, Yokohama, Kanagawa 230-0045, Japan

HIGHLIGHTS

- Our aim was to determine the design of support material for segmented-in-series SOFCs.
- We measured the changes in the Young's modulus with time.
- Young's modulus of ternary systems (i.e., Al_2O_3/TiO_2/MgO–NiO–YSZ) was measured.
- The behaviour of the Young's modulus depends on the framework composition of the sample.
- SEM analysis of the sample with a mirror polishing exhibits grain boundary sliding.

ARTICLE INFO

Article history:
Received 29 May 2013
Accepted 17 July 2013
Available online 25 July 2013

Keywords:
Solid oxide fuel cell
Segmented-in-series
Elastic modulus
Insulating material

ABSTRACT

As the substrate materials for segmented-in-series type solid oxide fuel cells (SOFCs), the mechanical characteristics, such as Young's modulus, of Al_2O_3–NiO–YSZ, TiO_2–NiO–YSZ and MgO–NiO–YSZ were examined under SOFC operating conditions. The Young's modulus for all of the samples decreased at a high temperature. For the Al_2O_3–NiO–YSZ samples, the behaviours of the Young's modulus changed at each process including as-sintered, 100 h reduction and 2000 h reduction. For the TiO_2–NiO–YSZ samples, the Young's modulus behaviour varied between the as-sintered and reduced samples. However, further reduction did not change the behaviour of the Young's modulus. For the MgO–NiO–YSZ samples, the Young's modulus of the samples exhibited a nearly constant behaviour through the sequence of processes from as-sintered to 100 h reduction and 2000 h reduction. Based on the microstructural analysis, the compositions of the framework of the samples and the sliding of the grain boundary strongly affected the Young's modulus.

1. Introduction

Fuel cells can directly convert chemical energy from fuels into electricity and achieve high-energy conversion efficiency compared to existing thermal power generation systems. In all of the fuel cell systems, solid oxide fuel cells (SOFCs) achieve the highest energy conversion efficiency, and they have been actively developed to utilise a limited quantity of fossil fuels [1,2]. Energy devices, such as SOFCs are expected to be operated for an ultra-long term period. The improvement in the power generation efficiency and generation capacity as well as the mechanical durability over an ultra-long term is a challenge for the commercial viability of SOFCs. In particular, understanding the mechanical properties under harsh operating conditions is important [3–8] because a SOFC's conventional operating temperature is very high (i.e., 700 °C–1000 °C).

As shown in Table 1, there are various types of SOFCs with different shapes and supporting substrates. Some authors have previously reported [9–11] that the segmented-in-series (SIS) type SOFCs based on electric insulating materials exhibit high durability against reduction and oxidation (Redox) cycles over a long period of operation. This result indicates that the SIS type SOFCs can be expected to have a long cell stack lifetime. These cell stacks constitute the main portions of the SOFC systems. Fig. 1 shows the schematic of an SIS type SOFCs. In the SIS type SOFCs, the substrate supports multiple single cells, and it has an important role as channels for the fuel supply. Therefore, substrates need to be strong with a high porosity. Because the substrate accounts for a large fraction of the cell stack volume, substrate damage results in breakage of cells. Therefore, understanding the mechanical behaviour is very important for designing substrate materials that exhibit ultra-long term durability. In particular, this substrate component is exposed

* Corresponding author. Tel.: +81 45 500 8820; fax: +81 45 500 8790.
E-mail address: somekawa@tokyo-gas.co.jp (T. Somekawa).

0378-7753/$ – see front matter © 2013 Elsevier B.V. All rights reserved.
http://dx.doi.org/10.1016/j.jpowsour.2013.07.071

Table 1
Classification of SOFCs.

Type	Substrate	Examples of manufacturing company
Planer type	Anode materials	Topsoe Fuel Cell A/S, SOFCpower, Versa Power Systems, Inc., Ceramic Fuel Cells Limited, NGK Spark Plug Co., Ltd., and more
	Porous metal	Ceres Power
	Electrolyte materials	Hexis Ltd., Bloom Energy Mitsubishi Materials Corporation
Cylindrical type	Anode materials	Acumentrics corporation, TOTO Ltd.
	Cathode materials	Siemens Westinghouse Power Corporation TOTO Ltd.
Flat tubular planer type	Electrical insulating materials	Mitsubishi Heavy Industries, Ltd.
	Anode materials	Kyocera Corporation
	Electrical insulating materials	Kyocera Corporation, Rolls-Royce plc

to a high temperature and reductive atmosphere for long periods. Therefore, understanding the mechanical property of the substrate materials and its variation with time are necessary [12,13].

In this study, we examined the mechanical property variations as a function of the reduction time of various types of substrate materials under SOFC operating conditions to determine the fundamental guiding principle for substrate material design. In detail, we measured the Young's modulus of ternary systems, such as Al_2O_3–NiO–YSZ (ANY), TiO_2–NiO–YSZ (TNY) and MgO–NiO–YSZ (MNY) at each step (i.e., as-sintered, 100 h reduction, and 2000 h reduction). We focused our attention on the Young's modulus because it exhibits a high correlation with internal stress [14–16] and is an important factor for evaluating the long-term reliability of SOFC cells.

2. Experimental setup

2.1. Sample preparation

The samples tested were manufactured from commercial ceramic powders using standard ceramic processing techniques. The sample compositions are shown in Table 2. The ternary systems including Al_2O_3–NiO–YSZ, TiO_2–NiO–YSZ and MgO–NiO–YSZ were prepared by physical mixing and agitating the powders of NiO (0.7 μm, Seido Chemical Industry Corp.), YSZ (1.9 μm, Daiichi Kigenso Kagaku Kogyo Co., Ltd.) and Al_2O_3 (0.3 μm, Sumitomo Chemical Co., Ltd.) or TiO_2 (2.0 μm, Koujundo Chemical Laboratory Co., Ltd.) or MgO, which was obtained by calcination of $Mg(OH)_2$ powders. As previously mentioned, because the substrate plays a role in fuel supply and needs to have a high porosity to ensure the fuel's diffusivity, a pore forming agent (microcrystalline cellulose type, Asahi Kasei Corp.) of 10 mass % was added to the mixture. A solution containing 10 mass % poly-vinyl butyral (BM-1, Sekisui Chemical Co.) in ethanol was added to prepare pellets without cracks. The powders were well mixed using an agate mortar and muddler for 30 min and pressed uniaxially into rectangular pellets with a 12 mm × 70 mm size at a pressure of 640 kg cm^{-2} for 60 s. The pellets were calcined at 1500 °C for 2 h. Then, the pellets were reduced at 800 °C in an atmosphere of 4% H_2 balanced N_2 for 100 h and 2000 h. After each process, we measured the porosity and Young's modulus and performed analyses using an X-ray diffractometer (XRD), a scanning electron microscope (SEM), and an energy dispersive spectroscopy (EDX).

Table 2
Sample details.

Sample name	Composition materials			Vol%			Mol%		
				NiO	YSZ	Al_2O_3, TiO_2, MgO	NiO	YSZ	Al_2O_3, TiO_2, MgO
ANY	NiO	YSZ	Al_2O_3,	30	35	35	47.8	28.1	24.1
TNY			TiO_2,				44.0	25.8	30.2
MNY			MgO				36.6	21.5	41.9

2.2. Experimental equipment

2.2.1. Measurement of Young's modulus

To measure the Young's modulus, a resonance method [17,18] was used in our study. In these measurements, the resonance frequencies of the samples were measured by setting one edge of the platy sample as the fixed end and the other as the free end. The Young's modulus was calculated by using Formula (1) and the measured resonance frequency.

$$E = \frac{4\pi^2 L^4 S\rho}{\alpha^2 I} f \tag{1}$$

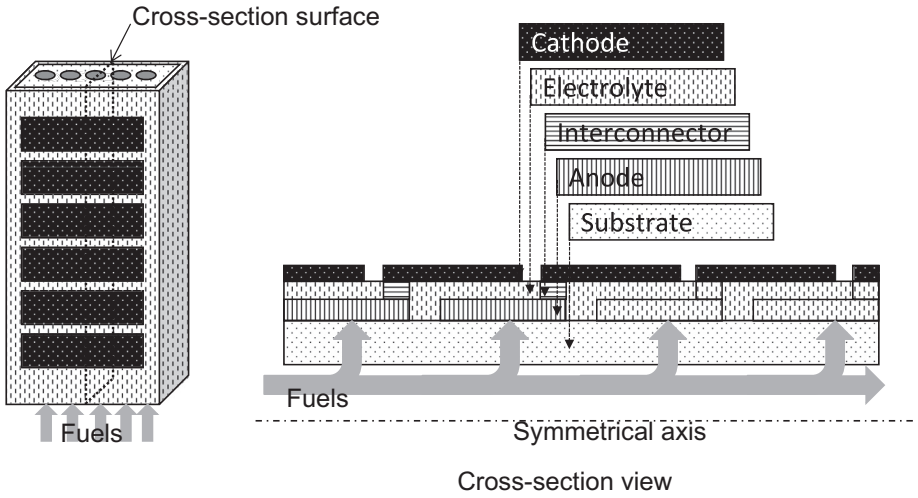

Fig. 1. Schematic of the SIS-type SOFCs.

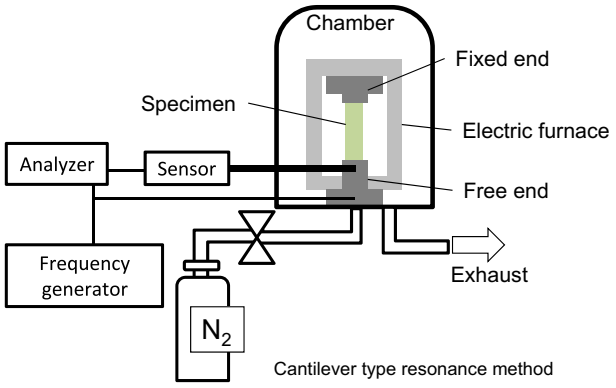

Fig. 2. Experimental set up for measurement of the Young's modulus.

Table 3
Porosity and Young's modulus of the samples at room temperature (25 °C).

Sample	ANY		TNY		MNY	
	Porosity Young's modulus		Porosity Young's modulus		Porosity Young's modulus	
	%	GPa	%	GPa	%	GPa
As-sintered	45.8	49.0	27.3	84.0	39.5	60.5
100 h reduction	50.5	35.0	33.2	68.5	37.5	58.8
2000 h reduction	49.7	34.7	31.9	67.5	38.8	64.0

where f is the resonance frequency, L is the length of sample, ρ is the density, S is the cross section area, I is the inertia moment, and α is the apparatus constant. Fig. 2 shows a schematic of the Young's modulus measurement equipment (Nihon Techno-Plus Co., Ltd., EG-HT). The as-sintered samples were measured in an air atmosphere, and the 100 h and 2000 h reduced samples were measured in an inert N_2 (50 mL min^{-1}) atmosphere. All of the samples were measured in the temperature ranges of room temperature (25 °C) to 1000 °C. And the porosity of the samples was measured by a helium pycnometer method (Micrometrics Instrument Corporation, AccuPyc1330).

2.2.2. XRD and SEM/EDX analysis

To analyse the compositions of the samples after each process, we measured the XRD patterns of the as-sintered sample as well as the 100 h and 2000 h reduced samples using an X-ray diffractometer equipped with a Cu target. To analyse the microstructural changes in the samples, the cross sections of each resined and polished sample were observed using a SEM/EDX (JEOL Ltd., EX-23000BU).

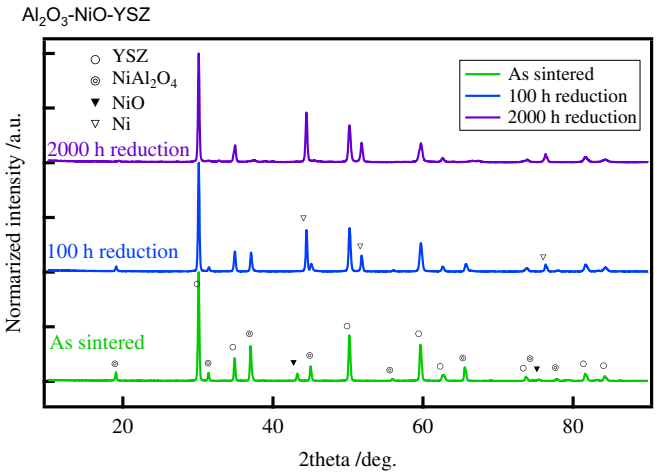

Fig. 4. XRD analysis of ANY.

3. Results and discussion

3.1. Results of the Young's modulus measurements

Table 3 shows the results of the porosity and Young's modulus measurements at room temperature (25 °C). The 100 h reduced ANY and TNY samples showed a decrease in Young's modulus because their porosity increased. Both the porosity and Young's modulus of 2000 h reduced ANY and TNY samples were nearly as same as those of the samples reduced for 100 h. This was because the reduction of all NiO into Ni with a volume change completed at the 100 h reduction process and the porosity didn't change in the further reduction. In MNY samples, all of the NiO dissolved into MgO and there was no volume change in the 100 h reduction and 2000 h reduction. And Young's modulus was almost constant in all the steps. These relationships between porosity and Young's modulus correspond to previous reports [5,19–21]. R.G. Munro reported [22] the Young's modulus can be given by the following Equation (2):

$$E = E_T(T)^* E_P(P) \quad (2)$$

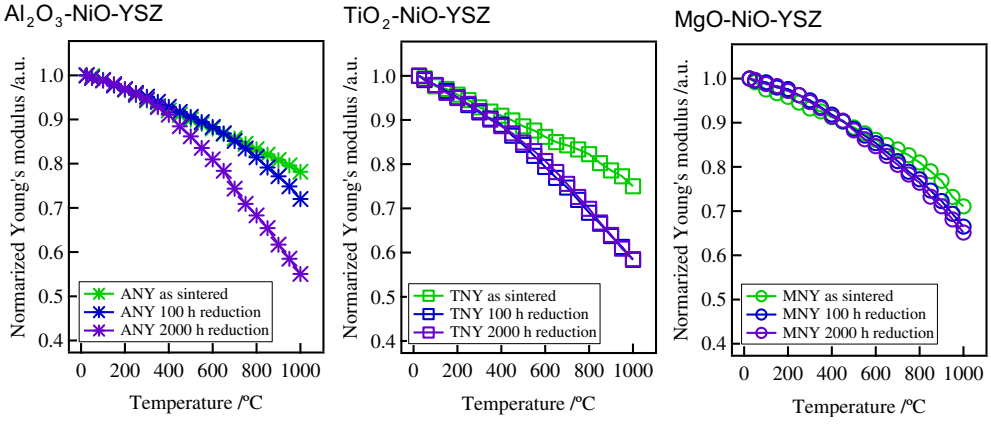

Fig. 3. Young's modulus for ANY, TNY and MNY.

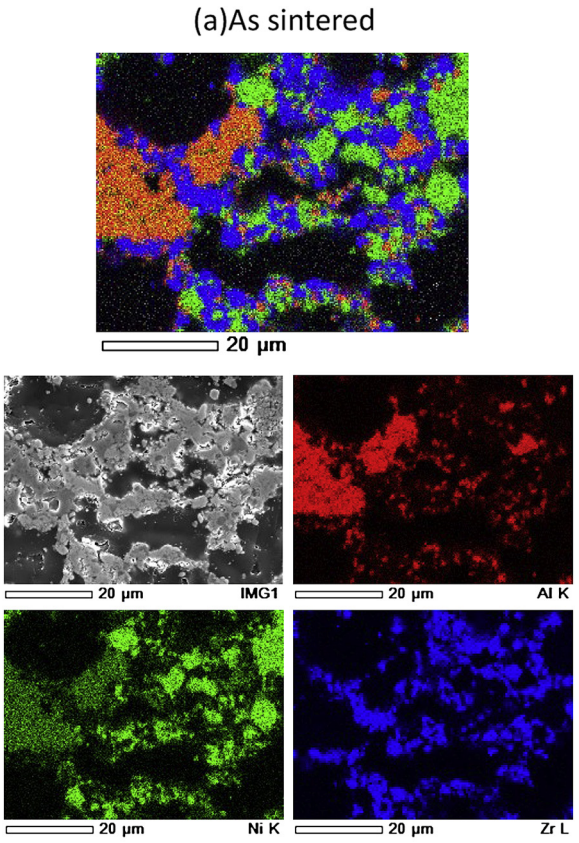

Fig. 5. SEM images and EDX results of the (a) as-sintered, (b) 100 h reduced and (c) 2000 h reduced ANY samples.

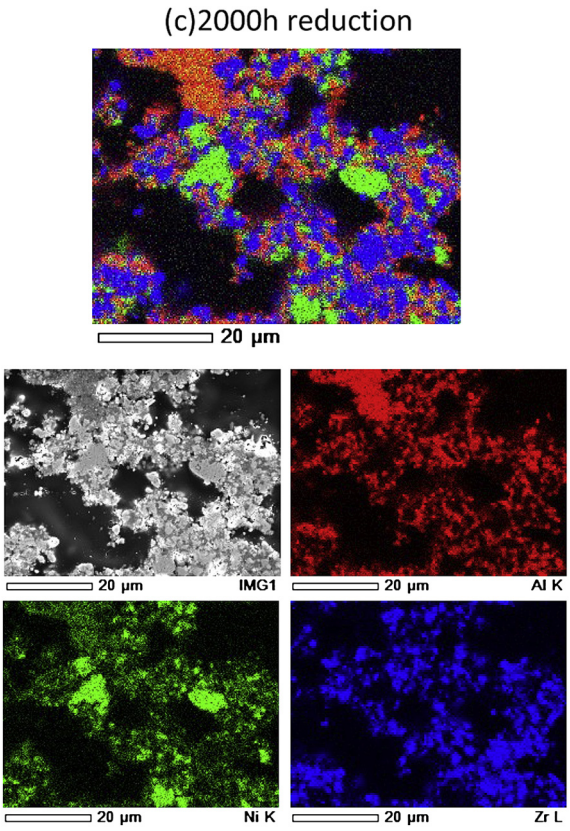

Fig. 5. (Continued)

where E is the Young's modulus, T is temperature, and P is porosity. This means that we can treat temperature dependence and porosity dependence in Young's modulus separately. And next we will show the temperature dependence in Young's modulus.

Fig. 3 shows the behaviour of the Young's modulus for the ANY, TNY, and MNY samples. In the graphs, the data were normalised by the values at room temperature (25 °C) to compare each result of the temperature dependence. All of the samples showed a decrease in the Young's modulus with temperature. The ANY samples exhibited different behaviours at each step (i.e., as-sintered condition, 100 h reduction, and 2000 h reduction). The behaviours of

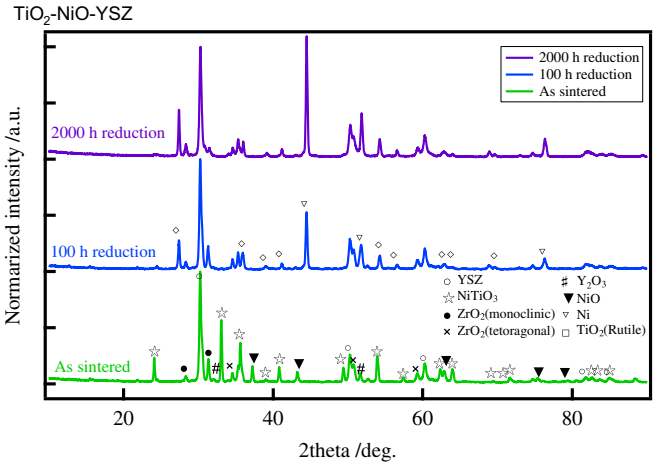

Fig. 6. XRD analysis of TNY.

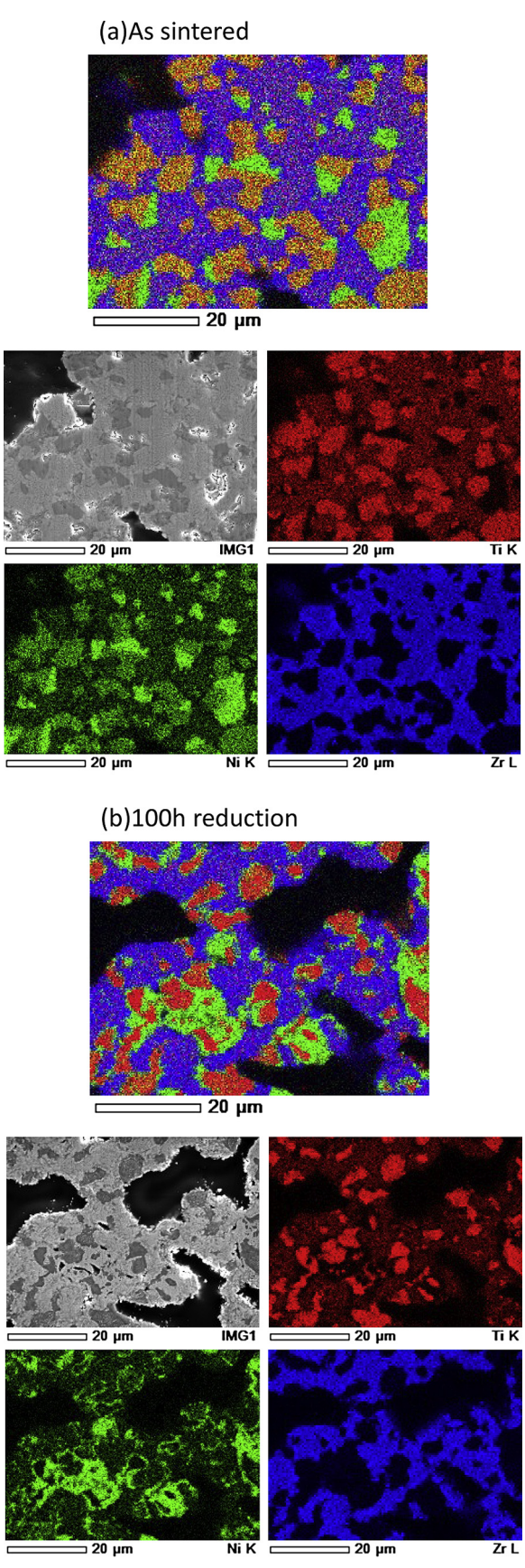

Fig. 7. SEM images and EDX results of the (a) as-sintered, (b) 100 h reduced and (c) 2000 h reduced TNY samples.

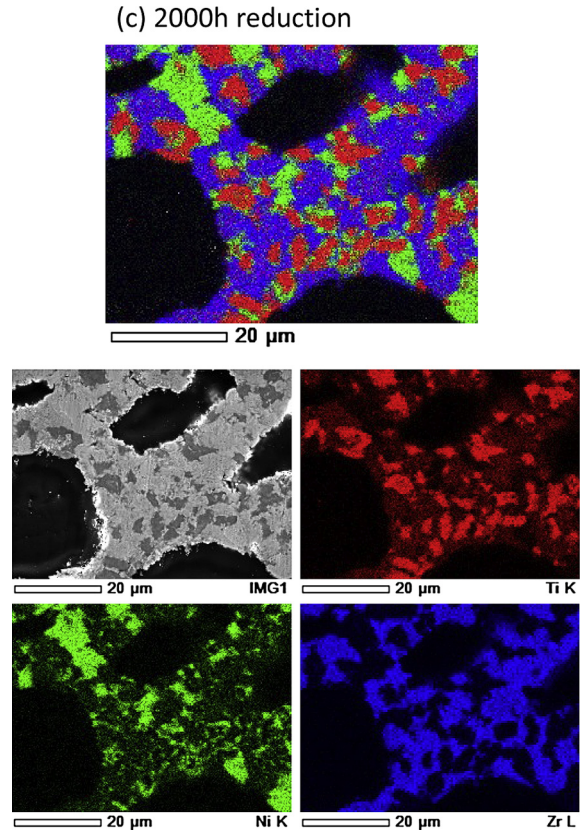

Fig. 7. (*Continued*).

TNY changed before and after reduction, but the prolonged reduction sample exhibited the same behaviour as the 100 h reduction sample. The MNY samples exhibited a nearly constant behaviour at each step.

3.2. XRD and SEM/EDX analysis results

3.2.1. Al_2O_3–NiO–YSZ

Fig. 4 shows the XRD analysis results of the ANY samples for the as-sintered, 100 h reduction, and 2000 h reduction samples. Initially, NiO and Al_2O_3 reacted to form $NiAl_2O_4$ via sintering. Then,

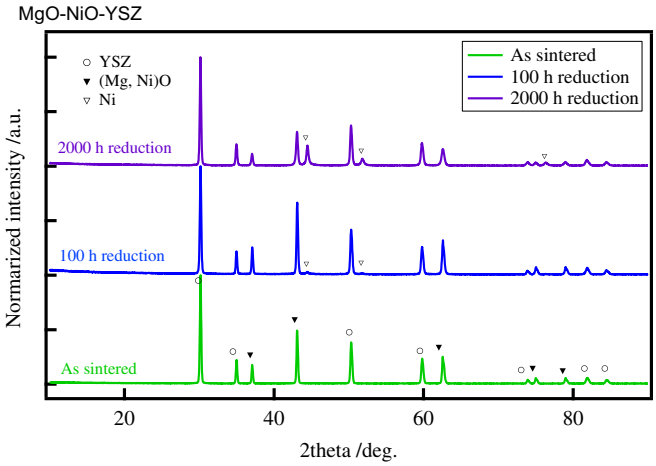

Fig. 8. XRD analysis of MNY.

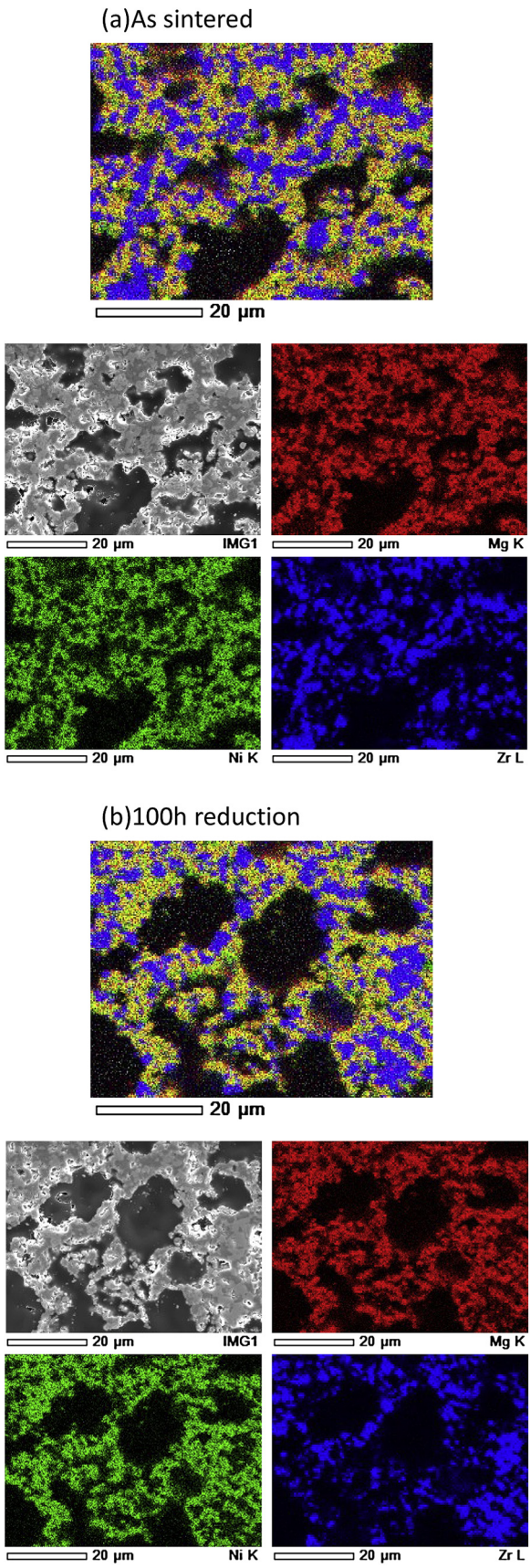

Fig. 9. SEM images and EDX results of the (a) as-sintered, (b) 100 h reduced and (c) 2000 h reduced MNY samples.

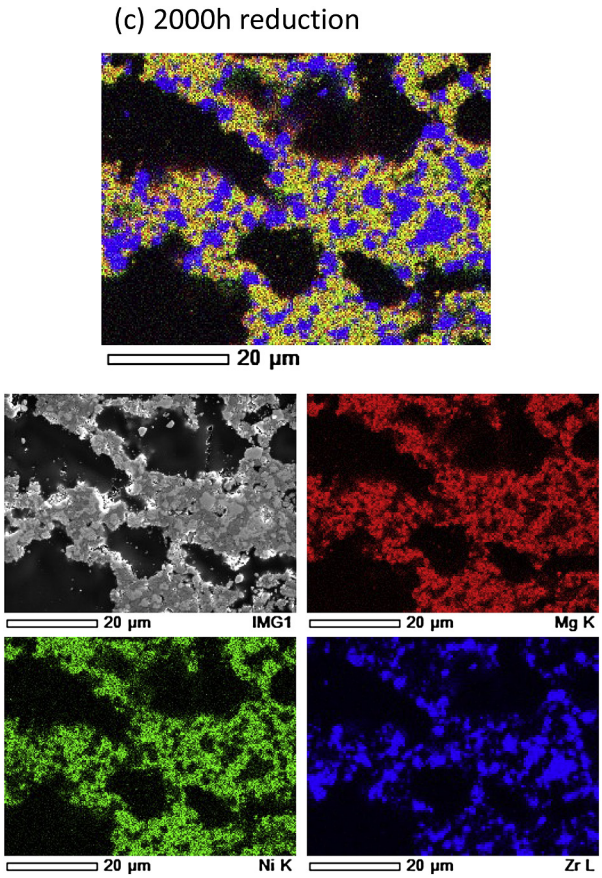

Fig. 9. (Continued)

the 100 h of reduction in 4% H_2 balanced N_2 resulted in the reduction of all of the NiO into Ni and portions of $NiAl_2O_4$ converted to Ni and Al_2O_3. Further reduction up to 2000 h completed the conversion of $NiAl_2O_4$ into Ni and Al_2O_3. Fig. 5 shows the SEM/EDX analysis of each processed samples. The EDX results showed that the framework of the as-sintered sample was composed of $NiAl_2O_4$–NiO–YSZ. In the 100 h reduced sample, the decomposition of $NiAl_2O_4$ was in the small amount, and it was assumed that the framework of the sample was composed of $NiAl_2O_4$–Ni–YSZ. In the 2000 h reduced sample, it was assumed that the framework of the sample was composed of Al_2O_3–Ni–YSZ because $NiAl_2O_4$ completely decomposed into Ni and Al_2O_3. Therefore, in the ANY samples, the materials that composed the macrostructures of the samples changed during the processes.

3.2.2. TiO_2–NiO–YSZ

Fig. 6 shows XRD analysis results from the TNY as-sintered, 100 h reduction, and 2000 h reduction samples. Initially, NiO and portions of the TiO_2 reacted to form $NiTiO_3$ via sintering, and portions of the TiO_2 dissolved into ZrO_2. Then, after the 100 h reduction, all of the NiO was reduced to Ni, and $NiTiO_3$ was completely converted to Ni and TiO_2. This result was determined based on the XRD patterns of the 100 h reduced sample, which exhibited no peaks associated with $NiTiO_3$. The XRD pattern of the extensively reduced sample was nearly the same as that of the sample reduced for 100 h, which indicated that extending the reduction time did not change the composition of the sample. Fig. 7 shows the SEM/EDX analysis of each processed samples. Based on the analysis, the framework of the as-sintered sample was composed of $NiTiO_3$–NiO–YSZ, and the framework of samples reduced for 100 h was composed of TiO_2–Ni–YSZ. In addition, the results from this analysis also indicated

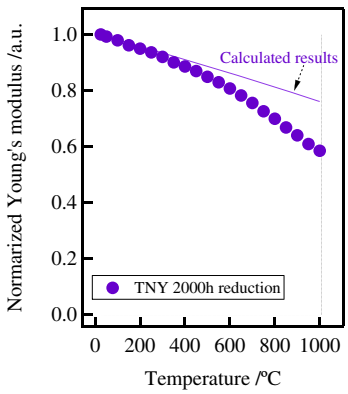

Fig. 10. Calculated Young's modulus for the TNY sample reduced for 2000 h.

that there were no structural changes for the compositions even after 2000 h of reduction.

3.2.3. MgO–NiO–YSZ

Fig. 8 shows the XRD analysis results for the MNY as-sintered, 100 h reduction, and 2000 h reduction samples. Initially, all of the NiO dissolved into the MgO, and a solid solution of (Mg, Ni)O was formed. After 100 h of reduction, nano-scale Ni particles segregated from the solid (Mg, Ni)O solution [23]. There were no compositional changes upon further reduction. Fig. 9 shows the SEM/EDX analysis of each processed sample. Based on the analysis, the framework of the as-sintered sample was composed of (Mg, Ni)O–YSZ. As previously mentioned, although nano-scale Ni particles segregated from (Mg, Ni)O after 100 h of reduction, the composition of the macrostructure did not change even after 2000 h of reduction.

Next, we will discuss the temperature dependence of the Young's modulus based on the results from the changes in the composition and microstructure. For the ANY samples, the behaviour of Young's modulus changed after reduction because the primary material of the macrostructure changed from $NiAl_2O_4$–NiO–YSZ to $NiAl_2O_4$–Ni–YSZ. Upon further reduction, the behaviour of the Young's modulus also changed, which may be due to the change in the framework composition members to Al_2O_3–Ni–YSZ. These results indicated that the behaviour of the Young's modulus strongly depends on the composition of the framework of the sample.

In an analogous way, the changes in the Young's modulus of the TNY samples between the as-sintered and reduced samples were due to the changes of the material of the framework from $NiTiO_3$–NiO–YSZ to TiO_2–Ni–YSZ. Further reduction did not change the behaviour of the Young's modulus because the framework of the samples reduced for 100 h and 2000 h were composed of the same materials. For the MNY samples, the behaviour of the Young's modulus did not change on going from the as-sintered sample to the sample reduced for 100 h, and 2000 h because in all of the steps, the framework of the samples were composed of (Mg, Ni)O–YSZ. Therefore, the behaviour of the Young's modulus strongly depends on the composition of the framework of the sample.

Next, we will discuss the differences between the previous empirical equation and the measured results. Some authors reported that a gradual temperature dependence of elastic modulus is typically seen with conventional ceramics and is due to decrease in the bonding strength caused by increase in atomic distance with increasing temperature, that is thermal expansion [24,25]. Previously, Ashby et al. reported [26] that the shear modulus empirically shows the temperature dependence given by the following equation:

$$\mu^* = \mu_0\left(1 + \frac{T - 300}{T_M}\left(\frac{T_M}{\mu_0}\frac{d\mu}{dT}\right)\right) \quad (3)$$

where μ_0 is the shear modulus at 300 K, $((T_M/\mu_0)^*(d\mu/dT))$ is the temperature dependence of the modulus, and T_M is the melting point. The Young's modulus is given by the following equation:

$$E = 2G(1 + \gamma) \quad (4)$$

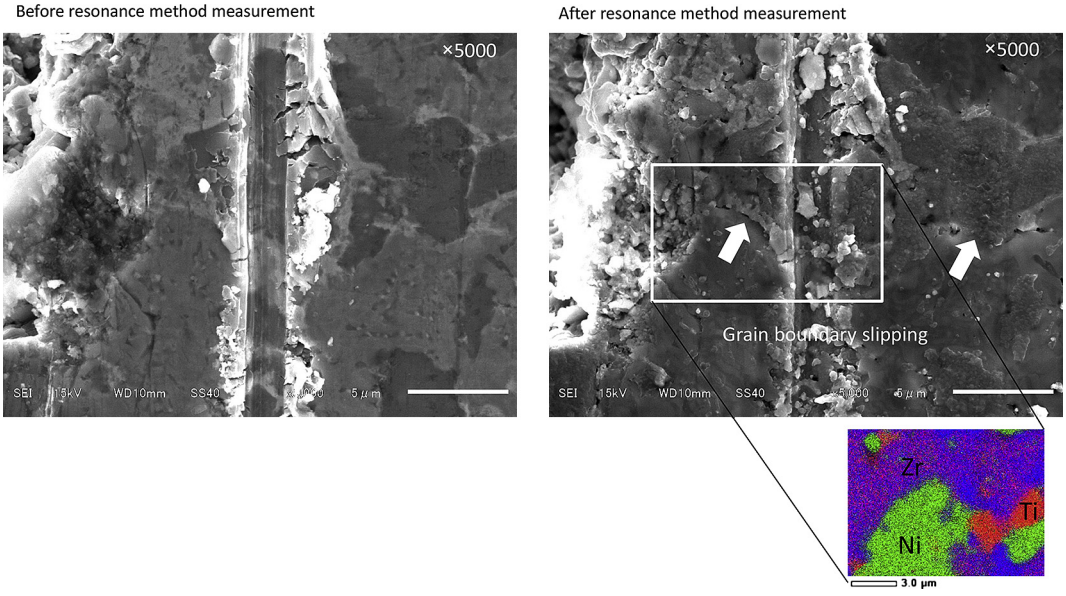

Fig. 11. SEM images of the sample before and after the resonance method measurement.

where G is the shear modulus, γ is the Poisson ratio. The Young's modulus for a sample composed of multiple materials was calculated using Equations (5) and (6).

$$E = E_1V_1 + E_2V_2 + \ldots + E_nV_n \quad (5)$$

$$\frac{1}{E} = \frac{V_1}{E_1} + \frac{V_2}{E_2} + \ldots + \frac{V_n}{E_n} \quad (6)$$

where E is the apparent Young's modulus, E_1, E_2,…, E_n are the Young's moduli of material 1, material 2,…, material n, and V_1, V_2,…, V_n are the volume fractions of material 1, material 2,…, material n. Equation (5) assumes an equal strain in all of the materials and provides an upper boundary of the Young's modulus, and Equation (6) assumes an equal stress in all of the materials and provides a lower boundary [27]. Fig. 10 shows the comparison between the calculated and measured values of the TNY sample reduced for 2000 h. Compared to the numerical results using equations from (3) to (6), the measured results exhibited a decrease in the Young's modulus as the temperature increased.

Fig. 11 shows the SEM images before and after the resonant method measurements of the 2000 h reduced TNY samples with a mirror polishing finish. In the sample, some scratches were introduced to identify SEM measuring locations. After the resonant method measurement, the analysis indicated that the sample exhibits slippage of the grain boundary, especially for the grain boundaries between Ni and YSZ. We are assuming that the grain boundary sliding actively occurred at high temperature resulting in the decrease in the Young's modulus.

4. Summary

We measured the changes in the Young's modulus of ternary systems (i.e., Al_2O_3–NiO–YSZ, TiO_2–NiO–YSZ, and MgO–NiO–YSZ) with time under SOFCs operating conditions to determine the guiding principle for design of substrate material with high mechanical reliability for SIS type SOFCs.

- In all of the samples, the Young's modulus decreased with high temperature.
- In the Al_2O_3–NiO–YSZ samples, the behaviour of the Young's modulus changed at each step in the process from as-sintered to sample reduction for 100 h and 2000 h.
- In the TiO_2–NiO–YSZ samples, the behaviour of the Young's modulus changed between the as-sintered and reduced samples. However, further reduction did not change the behaviour of the Young's modulus.
- For the MgO–NiO–YSZ samples, the Young's modulus exhibited nearly the same behaviour for all of the samples (i.e., as-sintered sample as well as samples reduced for 100 h and 2000 h).
- Microstructure analysis of the sample with a mirror polishing finish exhibits grain boundary sliding.
- It was assumed that the behaviour of the Young's modulus depends on the framework composition of the sample and grain boundary sliding.

References

[1] H. Yokokawa, ECS Trans. 35 (1) (2011) 207–216.
[2] K. Horiuchi, K. Nakamura, Y. Matsuzaki, S. Yamashita, T. Horita, H. Kishimoto, K. Yamaji, H. Yokokawa, ECS Trans. 35 (1) (2011) 217–223.
[3] S. Wang, H. Inaba, H. Tagawa, M. Dokiya, T. Hashimoto, Solid State Ionics 107 (1998) 73–79.
[4] S. Nakayama, S. Hashimoto, K. Sato, K. Yashiro, K. Amezawa, J. Mizusaki, ECS Trans. 25 (2) (2009) 1701–1708.
[5] S. Giraud, J. Canel, J. Eur. Ceram. Soc. 28 (2008) 77–83.
[6] J.W. Adams, R. Ruh, K.S. Mazdiyasni, J. Am. Ceram. Soc. 80 (1997) 903–908.
[7] Y. Du, N.M. Sammes, G.A. Tompsett, D. Zhang, J. Swan, M. Bowden, J. Electrochem. Soc. 150 (1) (2003) A74–A78.
[8] T. Kushi, K. Sato, A. Unemoto, S. Hashimoto, K. Amezawa, T. Kawada, J. Power Sources 196 (2011) 7989–7993.
[9] K. Fujita, T. Somekawa, T. Hatae, Y. Matsuzaki, J. Power Sources 196 (2011) 9022–9026.
[10] K. Fujita, T. Somekawa, K. Horiuchi, Y. Matsuzaki, J. Power Sources 193 (2009) 130–135.
[11] T. Somekawa, K. Fujita, Y. Matsuzaki, J. Power Sources 221 (2013) 64–69.
[12] T. Hahida, K. Sato, Y. Takeyama, T. Kawada, J. Mizusaki, ECS Trans. 25 (2) (2009) 1565–1572.
[13] F. Iguchi, Y. Endo, T. Ishida, T. Yokobori, H. Yugami, T. Otake, T. Kawada, J. Mizusaki, Solid State Ionics 176 (2005) 641.
[14] C.-H. Ma, J.-H. Huang, H. Chen, Thin Solid Films 418 (2002) 73–78.
[15] H. Yakave, Y. Baba, T. Sakurai, M. Satoh, I. Hirosawa, Y. Yoda, J. Power Sources 131 (2004) 278–284.
[16] H. Yakabe, Y. Baba, Y. Sakurai, J. Power Sources 135 (2004) 9–16.
[17] J. Spinner, W.E. Tefft, Proc. Am. Soc. Test. Mater. 61 (1961) 1221.
[18] U. Bayerlein, H.-G. Sockel, Mater. Sci. Eng. A 141 (1991) 179–187.
[19] A. Selcuk, A. Atkinson, J. Eur. Ceram. Soc. 17 (1997) 1523–1532.
[20] A. Atkinson, A. Selcuk, Solid State Ionics 134 (2000) 59–66.
[21] P. Mikko, K. Andress, M. Mogensen, J. Eur. Ceram. Soc. 29 (2009) 1657–1664.
[22] R.G. Munro, J. Res. Natl. Inst. Stand. Technol. 109 (2004) 497–503.
[23] T. Somekawa, K. Horiuchi, Y. Matsuzaki, J. Power Sources 202 (2012) 114–119.
[24] J.B. Watchman, W.E. Tefft, D.G. Lam, C.S. Apstein, Phys. Rev. 122 (1961) 1754–1759.
[25] O.L. Anderson, Phys. Rev. 144 (1966) 553–557.
[26] H.J. Frost, M.F. Ashby, Deformation-mechanism Maps, Pergamon Press, Oxford, UK, 1982.
[27] Hala A. Hafez, J. Mater. Sci. 16 (1981) 1223–1232.